Simulation study of a high performance brain PET system with dodecahedral geometry

Weijie Tao

School of Biomedical Engineering, Shanghai Jiao Tong University, Shanghai, China 200240

and Department of Nuclear Medicine, Ruijin Hospital, Shanghai, China 200240

Gaoyu Chen, Fenghua Weng

School of Biomedical Engineering, Shanghai Jiao Tong University, Shanghai, China 200240

Yunlong Zan

University of Michigan - Shanghai Jiao Tong University Joint Institute, Shanghai Jiao Tong University, Shanghai, China 200240

Zhixiang Zhao

School of Biomedical Engineering, Shanghai Jiao Tong University, Shanghai, China 200240

Qiyu Peng[a]

Lawrence Berkeley National Laboratory, Berkeley, USA 94720

Jianfeng Xu[a]

School of Mechanical Science and Engineering, Huazhong University of Science and Technology, Wuhan, Hubei, China 430074

Qiu Huang[a]

School of Biomedical Engineering, Shanghai Jiao Tong University, Shanghai, China 200240

and Department of Nuclear Medicine, Ruijin Hospital, Shanghai, China 200240

Abstract

Purpose: In brain imaging, the spherical PET system achieves the highest sensitivity when the solid angle is concerned. However it is not practical. In this work we designed an alternative sphere-like scanner, the dodecahedral scanner, which has a high sensitivity in imaging and a high feasibility to manufacture. We simulated this system and compared the performance with a few other dedicated brain PET systems.

Methods: Monte Carlo simulations were conducted to generate data of the dedicated brain PET system with the dodecahedral geometry (11 regular pentagon detectors). The data were then reconstructed using the in-house developed software with the fully three-dimensional maximum-likelihood expectation maximization (3D-MLEM) algorithm.

Results: Results show that the proposed system has a high sensitivity distribution for the whole field of view (FOV). With a depth-of-interaction (DOI) resolution around 6.67 mm, the proposed system achieves the spatial resolution of 1.98 mm. Our simulation study also shows that the proposed system improves the image contrast and reduces noise compared with a few other dedicated brain PET systems. Finally, simulations with the Hoffman phantom show the potential application of the proposed system in clinical applications.

Conclusions: In conclusion, the proposed dodecahedral PET system is potential for widespread applications in high-sensitivity, high-resolution PET imaging, to lower the injected dose.

Key words: Dodecahedral PET system, Monte Carlo simulation, system evaluation

1. INTRODUCTION

The application of dedicated brain Positron Emission Tomography (PET) system in brain imaging [1] dates back to almost two decades ago. Although different designs of PET systems such as hexagonal[2] and spherical[3] geometries have been proposed, the most popular clinical PET system is composed of detector modules of stacking rings.[4] The ring detector PET might

be a good choice for whole body imaging while not optimized for specific organs such as the brain, due to the low sensitivity. In order to increase image quality of the PET brain imaging,

30   dedicated brain PET systems were designed with small diameter detector rings, such as the High-Resolution Research Tomograph (HRRT) system[5,6] and the one with four-layer MPPC DOI detectors.[7,8] However, the sensitivity of these ring detector systems degrades heavily with the increase of the distance from axis in the transaxial plane.[9] The low sensitivity of the peripheral area in FOV affects quantitative accuracy for some brain regions, such as parts of

35   cerebellum region,[10] while the cerebellum region is vital for brain imaging because this region is usually used as the reference area.[11] In addition, the low sensitivity of these ring PET systems hampers the development of low-dose PET imaging.[12]

    Recently several designs of dedicated brain systems have been presented. Gong *et al*[13] simulated a helmet structure system that consists of six side rings with different diameters, a

40   top panel, and a bottom panel. A slightly different helmet PET was first presented and then upgraded to the helmet-chin system.[14-17] The scanner enhances the imaging performance for both bottom and top region of the brain. Moghaddam *et al*[18] designed a spherical brain PET system with liquid xenon detectors, with a large solid angle[19] but much complexity in realization in practice. Our previous study[20] has assessed different geometric brain PET

45   systems with large solid angels and found that the dodecahedral PET was a reasonable approximation of the spherical cap PET.

    In this study, we simulated this dedicated brain PET system with the dodecahedral geometry using the GATE toolkit.[21] The system performance has been evaluated in term of sensitivity, spatial resolution, count rate and reconstructed image quality, compared to the

50   helmet system designed by Gong *et al*,[13] the helmet-chin PET proposed by Ahmed *et al*,[17] and the HRRT brain PET system.[5]

2. MATERIALS AND METHODS

2.A. System design

55   The dedicated dodecahedral brain PET scanner consists of 11 flat depth-of-interaction (DOI) detector modules and an open face, as shown in Fig. 1. All detector modules and the open face are pentagons of the same size. The inscribed circle of the pentagon has a radius being 9.28

cm. The dodecahedron has an inscribed sphere with radius 15 cm. In other words, the distance from the center to each detector plane is 15 cm, which makes every two opposite modules 30

60 cm apart. The circumradius of dodecahedron is 18.8 cm so that the longest distance between two points in the scanner does not exceed 37.6 cm. The detectors consist of high-density pixelated-LYSO crystals with the size of 2 mm × 2 mm × 20 mm (thickness). All simulation parameters are summarized in Table I.

   We constructed the structure of dodecahedron in GATE v7.1 with the 'generic repeater'

65 function and analyzed the simulated data in the ROOT program package.[22] In all simulations of the dodecahedral scanner, unless otherwise specified, the energy window was chosen to be 250-750 keV with the energy resolution being 14%, and the coincidence timing window was 6 ns. Parallax errors affect spatial resolution[23] even at the center of the proposed system since gamma rays emitted from the center may enter crystals obliquely. We added the DOI

70 information to reduce the parallax error.[24]

2.B. Phantoms

   To evaluate the performance of our proposed brain system, we simulated six phantoms to be consistent with those for the helmet system,[13] the helmet-chin PET,[17] and the HRRT

75 system.[5] Table II lists all six phantoms. The first three of them were directly defined in GATE. The uniform water cylinder phantom, with a diameter of 24.5 cm and the axial length of 19 cm,[13] was used for comparison of sensitivity. And a hemisphere phantom with a diameter of 22.8 cm[17] was used to assess the noise equivalent count rate (NECR). Besides, the point source phantom was designed to measure the resolution at different positions in the FOV. It

80 consists of 19 radioactive point sources either placed along the positive X-axis in the plane Z=0 cm or along the Z-axis. All point sources have a diameter of 1 mm, and are 2 cm apart from the adjacent source. The last three phantoms, Derenzo phantom, Jaszczak phantom,[25] and Hoffman phantom,[26] were imported into GATE.

2.C. Image reconstruction

85

   The simulated PET data were reconstructed using our in-house developed reconstruction software. The software was developed according to the fully three-dimensional

maximum-likelihood expectation maximization (3D-MLEM) algorithm on list mode data.[27] We have validated our software via reconstructions of images for the ECAT[28] and mCT[29] systems using Software for Tomographic Image Reconstruction (STIR)[30] as the benchmark. Throughout this study, 20 iterations were used in the reconstruction. The matrix size of reconstructed images was set to $256 \times 256 \times 250$ with a voxel size of $1 \times 1 \times 1$ mm^3 except for the Hoffman phantom, which has a matrix size of $240 \times 240 \times 80$ with a voxel size of $1 \times 1 \times 2.5$ mm^3.

2.D. Performance assessment

The system performance was evaluated using a few metrics explained in this subsection. In order to compare the proposed system with the commercialized system HRRT, we also simulated HRRT with the exact same physics model and calculated these metrics. However, for the helmet and helmet-chin systems, due to their complicated geometries, we referred to figures of merit in literatures.

2.D.1. Sensitivity

The overall sensitivity performance was evaluated using the uniform water cylinder phantom (as in Table II) injected with 1 MBq ^{18}F-FDG. The phantom was positioned in the center of the FOV with its axis along Z-axis. In GATE simulation, true and scattered events were recorded separately. We then obtained the overall sensitivity as the ratio between the number of detected true events and the total number of annihilations in the phantom.

To illustrate the uniformity of sensitivity, the point source was positioned in each voxel of a water sphere with diameter 26 cm, and then spatial sensitivity maps were obtained by calculating the sensitivity at each voxel for planes at specific Z-axis coordinates.

2.D.2. Resolution

Spatial resolution represents the ability of the system to resolve small objects. Two approaches were used to assess the spatial resolution. One measured the size of the reconstructed image of a point source. After the image of the point source was reconstructed and fit with a Gaussian function, the full width at half maximum (FWHM) of the Gaussian function was calculated as the metric. In this study, we used the point source phantom containing 19 points as described in Section 2.B. The other approach used the visual

observation on the image of a modified Derenzo phantom. We simulated an injection of 5.7

MBq ^{18}F-FDG with acquisition time being 10 s for this phantom introduced in Table II.

2.D.3. Noise equivalent count rate (NECR)

The NECR of the scanner provides a global measure of the noise performance of the

system, since it is not sensitive to regional variations of the source distribution. As in the

helmet-chin PET study,[17] NECR was assessed using the hemispherical phantom and the

energy window was set as 400-600 keV. At a fixed activity, NECR was calculated using the

formula given by Strother *et al*:[31]

$$NECR = \frac{T^2}{T+S+2R} \tag{1}$$

where T, S and R are the true, scatter and random count rates, respectively.

2.D.4. Contrast-to-noise ratio (CNR) and contrast recovery coefficient (CRC)

Noise property in the reconstructed image is essential to clinical practice. To compare the

means of CNR and CRC for different systems using the Jaszczak phantom (as in Table II), we

simulated an injection of 7 MBq ^{18}F-FDG with acquisition time being 100 s in GATE. The

activity concentrations were 3:1 for the hot spheres and the background. In the reconstructed

PET images, two types of regions of interest (ROIs) were drawn. One was placed in the

background of the image. And the other was placed inside the hot area, covering the entire

area of the hot spot. The activity difference between these two ROIs was then normalized by

the standard deviation of the background to represent the noise level in the reconstructed

images, a.k.a, the contrast-to-noise ratio. Thus CNR is represented as

$$CNR = \frac{M_{ROI}-M_{BG}}{NSD} \tag{2}$$

where M_{ROI} and M_{BG} are the evaluated mean activity concentration in the hot ROI and the

background ROI, and NSD is the standard deviation of the background ROI.[32]

CRC is quantified by the percent contrast for each hot ROI as:

$$CRC = \frac{M_{ROI}/M_{BG}-1}{\alpha_{ROI}/\alpha_{BG}-1} \times 100\% \tag{3}$$

where α_{ROI} and α_{BG} are the mean activity concentrations in the hot spheres and background.[5]

3. RESULTS

3.A. Comparison of sensitivity

The overall sensitivity performance is shown in Table III for the proposed system, together with the HRRT system and the helmet PET system[13]. According to the result, our proposed PET system has an improvement in the sensitivity by 72% compared with the helmet system

150   and by 4.91 times compared with the cylinder brain scanner. The scatter fractions of the three systems are also shown in Table III. The result shows that the dodecahedral brain PET has higher scatter fraction respect to the helmet system. This is due to the larger solid angle and smaller solid space of the dodecahedral system.

The spatial sensitivity map is shown in Fig. 2 for six axial planes in the whole FOV of the

155   proposed system. In each transaxial plane, the sensitivity is higher at the edge than in the center section, while higher uniformity is evident in the center region. This is due to the attenuation of the sphere water phantom. As expected, sensitivity decreases along the Z-axis, since the open flat was located at Z=15 cm. Standard deviation of each slice was calculated to assess the uniformity along the Z-axis. As shown in Fig. 3, higher variation is observed in the

160   transaxial planes closer to the open flat.

3.B. Spatial resolution

To evaluate spatial resolution of the proposed system, we first calculated the FWHM of reconstructed point sources. Due to the high parallax errors of the compact design, the spatial

165   resolution is worse than 2.4 mm. We then included the DOI information to reduce the parallax errors. For DOI detectors, the crystals were divided into multiple layers in the radial direction with equal lengths. We compared FWHM along three directions with DOI resolutions being 20, 10, 6.67, and 5 mm, corresponding to 1, 2, 3, and 4 layers of crystals. Results are shown separately for points along Z-axis (Figs. 4(a), (c) and (e)) and along X-axis (Figs. 4(b), (d) and

170   (f)) in the center plane. It is evident that the more the layers, the better resolution the system achieves. When the DOI resolution is designed to be 6.67 mm, the best spatial resolution of our dedicated brain system is achieved near the center of the FOV, which is 1.98 mm, better than the helmet-chin system (2.5 mm with DOI resolution being 5 mm)[16] and the HRRT system (2.5 mm with DOI resolution being 10 mm).[5] We then chose DOI resolution of 6.67

175   mm for simulations in the rest of this work.

To assess the spatial resolution via the Derenzo phantom, Fig. 5 shows the center slice of

the reconstructed images where each voxel has been normalized to the maximum activity in the image. Our dodecahedral system and the HRRT system are both able to distinguish the smallest rods with the diameter of 2.4 mm, which is better than that of the helmet system (2.7 mm).[13] The profile shows that our system resolves the smallest rods better than the HRRT system.

3.C. NECR

The NECR curves of the HRRT system and of our proposed system are reported in Fig. 6. The peak-NECR for HRRT is 307.1 kcps when the phantom is filled with a uniformly distributed activity of 117.5 MBq. The peak-NECR of the dodecahedral system is 691.2 kcps at 258 MBq. The helmet-chin PET has the peak-NECR values of 265 kcps at 55 MBq.[17] Comparison of the peak-NECR is listed in Table IV. Our dodecahedral scanner increases the peak-NECR by 1.61 times compared to the helmet-chin scanner and by 1.25 times compared to the HRRT scanner.

3.D. CNR and CRC evaluations

CNR values were calculated using Eq. (2) for 6 hot ROIs indicated by red circles in Fig. 7(a), where the background ROI, as in blue in Fig. 7(a), was chosen to be the disk with 48 mm in diameter at the center of the Jaszczak phantom. Fig. 7(b) shows CNRs of the 6 ROIs for the dodecahedral system and the HRRT system. The proposed dodecahedral system has an average improvement in CNR by 74% compared with the HRRT system.

The percentage CRCs of 6 ROIs are listed in Table V. The dodecahedral system shows better ability of contrast recovery, compared to HRRT.

3.E. Potential Clinical Application

To illustrate the potential clinical application of our proposed system, a 3D Hoffman phantom was imported into the GATE toolkit to coordinate the activity distribution with the brain regions. The digital phantom was segmented into 116 volumes of interest (VOIs) based on magnetic resonance images. The average sensitivity of each VOIs of the Hoffman brain phantom was calculated and then the average values were mapped to each corresponding

brain regions to obtain the sensitivity map. The sensitivity map of cross section, sagittal plane and coronal plane were shown in Fig. 8. The average sensitivity around 9% can be observed in brain regions corresponding to a lot of common brain diseases, for instance, the angular gyrus, parietal lobe, occipital lobe and frontal lobe. The high sensitivity indicates that with the proposed system higher sensitivity (or lower dosage) may be possible in diagnose of some brain diseases such as Alzheimer and Parkinson. Besides, we planned to integrate the system with virtual reality goggles to image patients with claustrophobia and to perform other cognitive studies.

For the Hoffman phantom data, we simulated an injection of 2.67 MBq ^{18}F-FDG with acquisition time being 1000 s. Fig. 9 compares three representative (top, middle and bottom) slices of the Hoffman phantom reconstructions for the dodecahedral PET system and the HRRT system. For all slices, the dodecahedral PET produces images with lower noise than the HRRT system. This is consistent with the sensitivity improvement.

4. DISCUSSION

This work simulated a high-sensitivity brain PET system. The system has a great improvement in sensitivity respect to the HRRT system and the helmet system.[13] The peak NECR of the proposed system is significantly improved compared to the HRRT system and the helmet-chin system[14] (see Table IV) due to the increased sensitivity. The CRC of our proposed system is slightly better than that of the HRRT system. Furthermore, the dodecahedral system provides images with less noise than the HRRT system and shows higher CNR values. Though a detailed comparison will be conducted in the future, based on our simulation, we notice that the dodecahedral system also outperforms the brain PET with four-layer MPPC DOI detectors in terms of sensitivity,[8] since the latter (2.14%) has lower sensitivity than the HRRT system (2.5%).[6]

For a compact design such as the dodecahedral system, DOI information is critical to the image quality. The HRRT system used 10 mm LSO and 10 mm LYSO for DOI; the helmet-chin system used 4 layers in the 20 mm crystal; and Gong *et al*[13] simulated the helmet system with 3 layers of crystal, which made the DOI resolution 6.67 mm; the ring PET[8] with 4-layer MPPC DOI detectors was designed with crystal lengths 3, 4, 5 and 8 mm for each

layer. In our resolution comparison (Fig. 4 and 5), when the DOI resolution is 6.67 mm, the dodecahedral system achieves a slightly better spatial resolution than the HRRT, helmet, and helmet-chin systems. Thus we chose this three-layer DOI in other simulations. However, the

240   ring PET[8] with 4-layer MPPC DOI detectors shows even better resolution thanks to the smaller crystal sectional area (1.2×1.2 mm^2) and the shorter crystal lengths.

In order for a fair comparison, we simulated both HRRT and the dodecahedral system in GATE. However, the simulations of the helmet and helmet-chin geometries are not trivial. We thus only borrowed results from literatures. Meanwhile, for HRRT and the dodecahedral

245   system, we simulated the same phantom and matched the acquisition conditions as in those literatures. For instance, when comparing overall sensitivity, we simulated a big cylinder water phantom to be consistent with the one in *Gong et al.*[13] This is different from what is suggested by NEMA and resulted in lower sensitivity for the HRRT system than that in Sossi *et al.*[5] When NECR was concerned, the same scenario was simulated as in the helmet-chin

250   PET, which used a hemisphere with a radius of 114 mm instead of line sources. With different phantoms, the value is different while the trend is similar. For instance, the trend of CRC values for HRRT agree with that in Sossi *et al.*[5]

This work provided detailed simulations for a brain PET system under construction. There are a few issues to be improved both in software design and hardware design. Images in

255   Figs. 5, 7 and 9 were reconstructed with all detected events in the energy window of 250-750 keV, including true and scattered events. For both HRRT and the proposed system, no scatter correction has been done in this work. While scatter correction is necessary given the high fraction of scattering photons. Meanwhile, the scanner is simulated with pixelated crystals of 2 mm, which limits the spatial resolution of the reconstructed images. We plan to use

260   monolithic crystals to further improve the resolution and compare the performance with the 4-layer MPPC PET.

5. CONCLUSION

We have performed simulation studies to evaluate the performance of a dodecahedral PET

265   scanner for brain imaging and compared it with three other dedicated brain PET scanners. Our study shows that the proposed system improves the overall sensitivity by a factor of 4.91

compared with the cylindrical brain PET system (e.g., HRRT) and by a factor of 72% compared with the helmet system designed by Gong *et al*. The proposed system also increases the peak-NECR by 1.61 times compared to the helmet-chin scanner and by 1.25 times compared to the HRRT scanner. Reconstructed phantom images demonstrated high image quality with DOI information. With a DOI resolution being 6.67 mm, the proposed system achieves best spatial resolution of 1.98 mm near the center, better contrast recovery ability, and higher contrast-to-noise-ratio than the HRRT system. Using a Hoffman phantom we also demonstrated the potential clinical application of the proposed system.

ACKNOWLEDGMENT

[a)]Author to whom correspondence should be addressed. Electronic address: qpeng@lbl.gov, jfxu@hust.edu.cn and qiuhuang@sjtu.edu.cn

[1] Cho Z. H., Son Y. D., Choi E. J., Kim H. K., Kim J. H., Lee S. Y., et al, "In-vivo human brain molecular imaging with a brain-dedicated PET/MRI system," Magn. Reson. Mater. Phy., **26**(1), 71-79 (2013)

[2] Karp J. S., Surti S., Freifelder R., Daube-Witherspoon M. E., Cardi C., Adam L. E., et al, "Performance of a GSO brain PET camera," Nuclear Science Symposium Conference Record 2000:17/7-1711 vol.3.

[3] Cho Z. H., Hong K. S., Hilal S. K, "Spherical positron emission tomograph (S-PET) I - performance analysis," Nucl. Instrum. Methods Phys. Res. **225**(2), 422-438 (1984).

[4] Reske S. N., Kotzerke J., "FDG-PET for clinical use," Eur. J. Nucl. Med., **28**(11), 1707-1723 (2001).

[5] Sossi V., De Jong H. W. A. M., Barker W. C., Bloomfield P., "The second generation HRRT - a multi-centre scanner performance investigation," Nuclear Science Symposium Conference Record 2005:2195-2199.

[6] De Jong H. W., Van Velden F. H., Kloet R. W., Buijs F. L., Boellaard R., Lammertsma A. A., "Performance evaluation of the ECAT HRRT: an LSO-LYSO double layer high resolution, high sensitivity scanner," Phys. Med. Biol., **52**(5),1505-1526 (2007).

[7] Omura T., Moriya T., Yamada R., Yamauchi H., Saito A., Sakai T., et al, "Development of a high-resolution four-layer DOI detector using MPPCs for brain PET," Nuclear Science Symposium and Medical Imaging Conference. 2012:3560-3563.

300 [8] Watanabe M., Saito A., Isobe T., Ote K., Yamada R., Moriya T. Omura T., "Performance evaluation of a high-resolution brain PET scanner using four-layer MPPC DOI detectors," Phys. Med. Biol., **62**(17),7148 (2017).

[9] Pajak M. Z., Volgyes D., Pimlott S. L., Salvador C. C., Asensi A. S., Mckeown C., et al, "NEMA NU4-2008 Performance Evaluation of Albira: A Two-Ring Small-Animal PET System Using

305 Continuous LYSO Crystals," Open Med. J. **3**(1), 12-26 (2016).

[10] Son Y. D., Kim H. K., Kim S. T., Kim N. B., Kim Y. B., Cho Z. H., "Analysis of biased PET images caused by inaccurate attenuation coefficients," J. Nucl. Med. **51**(5), 753-60 (2010).

[11] Pickut B. A., Dierckx R. A., Dobbeleir A., Audenaert K., Van L. K., Vervaet A., et al, "Validation of the cerebellum as a reference region for SPECT quantification in patients suffering from dementia of

310 the Alzheimer type," Psychiatry Res. **90**(2), 103-112 (1999).

[12] Chatziioannou A., Dahlbom M., "Study of the effects of whole body PET spatial sampling schemes on data SNR," Nuclear Science Symposium Conference Record 2002:1295-1299 vol.2.

[13] Gong K., Majewski S., Kinahan P. E., Harrison R. L., Elston B. F., Manjeshwar R., et al, "Designing a compact high performance brain PET scanner-simulation study," Phys. Med. Biol. **61**(10), 3681

315 (2016).

[14] Tashima H., Yoshida E., Nishikido F., Wakizaka H., Nitta M., Ahmed A. M., et al, "Development of the helmet-chin PET prototype," Nuclear Science Symposium and Medical Imaging Conference 2016:1-3.

[15] Tashima H., Yamaya T., "Proposed helmet pet geometries with add-on detectors for high sensitivity

320 brain imaging," Phys. Med. Biol. **61**(19), 7205 (2016).

[16] Ahmed A. M., Tashima H., Yoshida E., Yamaya T., "Investigation of the optimal detector arrangement for the helmet-chin PET – A simulation study" Nucl. Instrum. Methods Phys. Res. **858**, 96-100 (2017).

[17] Ahmed A. M., Tashima H., Yoshida E., Nishikido F., Yamaya T., "Simulation study comparing the

325 helmet-chin PET with a cylindrical PET of the same number of detectors," Phys. Med. Biol. **62**(11), 4541 (2017).

[18] Moghaddam N. M., Karimian A., Mostajaboddavati S. M., Vondervoort E., Sossi V, "Preliminary design and simulation of a spherical brain PET system (SBPET) with liquid xenon as scintillator," Nukleonika **54**(1), 33-38 (2009).

330   [19] Bao Q., Cho S. and Li Q., Newport D., "Monte Carlo based estimation of detector response in a large solid angle Preclinical PET imaging system," IEEE Nuclear Science Symposium Conference Record 2008:5010-5013.

[20] Shi H., Du D., Xu J., Su Z., Peng Q., "Design study of dedicated brain PET with polyhedron geometry," Technol. Health Care **23** Suppl2(S2), S615 (2015).

335   [21] Jan S., Santin G., Strul D., Staelens S., Assié K, Autret D., et al, "Gate: a simulation toolkit for PET and SPECT," Phys. Med. Biol. **49**(19), 4543 (2004).

[22] Rademakers F., Brun R., "ROOT: an object-oriented data analysis framework," Nucl. Instrum. Methods Phys. Res. **389**(1-2), 81 -86 (1998).

[23] Kao C. M., Dong Y., Xie Q., "Evaluation of 3D image reconstruction methods for a dual-head

340   small-animal PET scanner," Nuclear Science Symposium Conference Record 2008:3046-3050.

[24] Kao C. M., Pan X., Chen C. T., "Accurate image reconstruction using DOI information and its implications for the development of compact PET systems," IEEE T. Nucl. Sci. **47**(4), 1551-1560 (2002).

[25] Jaszczak, "Nuclear imaging phantom" US 4499375 A (1985).

345   [26] Hoffman E. J., Cutler P. D., Digby W. M., Mazziotta J. C., "3-D phantom to simulate cerebral blood flow and metabolic images for PET," 1990:616-620.

[27] Huesman R. H., Klein G. J., Moses W. W., Qi J., "List-mode maximum-likelihood reconstruction applied to positron emission mammography (PEM) with irregular sampling," IEEE T. Med. Ima., **19**(5), 532-7, (2000).

350   [28] Jan S., Comtat C., Strul D., Stantin G. and Trebossen R., "Monte Carlo Simulation for the ECAT EXACT HR+ system using GATE," T. Nucl. Sci., **52**(3):627-633 (2005).

[29] Rausch I., Cal-González J., Dapra D., Gallowitsch H. J., Lind P., Beyer T., et al, "Performance evaluation of the Biograph mCT Flow PET/CT system according to the NEMA NU2-2012 standard," Ejnmmi Physics, **2**(1):1-17 (2015).

355   [30] Thielemans K, Tsoumpas C. and Mustafovic S, Beisel T., Aguiar P., Dikaios N. and Jacobson M. W., "STIR: software for tomographic image reconstruction release 2," Nuclear Science Symposium

Conference Record IEEE, 2174-2176 (2012).

[31] Strother S. C., Casey M. E., Hoffman E. J., "Measuring PET scanner sensitivity: relating countrates to image signal-to-noise ratios using noise equivalents counts," IEEE T. Nucl. Sci. **37**(2), 783-788 (1990).

[32] Hart H. J., Bottomley P. A., Edelstein W. A., Karr S. G., Leue W. M., Mueller O., et al, "Nuclear magnetic resonance imaging: contrast-to-noise ratio as a function of strength of magnetic field," Magn. Reson. Imaging **2**(6), 1195 (1983).

FIG. 1. Geometry of the proposed dodecahedral scanner.

FIG. 2. The distribution of sensitivity in ROI. (a) z=1 cm and z=-1 cm. (b) z=5 cm and z=-5 cm. (c) z=10 cm and z=-10 cm.

FIG. 3. Standard deviation of sensitivity.

FIG. 4. Effect of DOI on spatial resolution. The first column (a, c, and e) shows FWHM for points along Z-axis, while the second column (b, d, and f) for points along X-axis at Z=0. From top to bottom, each row shows FWHM along radial, tangential and axial directions, respectively.

FIG. 5. The reconstructed images for Derenzo phantom from the HRRT system and the dodecahedral system. (a) The center slice for the HRRT system. (b) Profile along the blue line

in (a) corresponding to the hot rods with diameter of 5.0 mm (peaks on the left) and 2.4 mm (peaks on the right). (c) The center slice for the dodecahedral system. (d) Profile along the blue line in (c) corresponding to the hot rods with diameter of 5.0 mm (peaks on the left) and

390   2.4 mm (peaks on the right).

FIG. 6. NECR curves of the HRRT system and the dodecahedral system.

FIG. 7. Comparison of CNR between the dodecahedral system and the HRRT system. (a) ROIs in the hot regions (red circles with diameters of 14.4 mm, 19.2 mm, 27.2 mm, 33.6 mm, 43.2 mm, 59.2 mm) and in the background (blue circle with diameter of 48 mm). (b) CNR for

395   the six ROIs in the HRRT system and the dodecahedral system.

FIG. 8. Three perspectives on the sensitivity of brain regions. (a) Cross section of the brain. (b) Sagittal plane of the brain. (c) Coronal plane of the brain.

FIG. 9. The reconstructed images of the Hoffman phantom for the HRRT system (top row) and the dodecahedral system (bottom row). (a) Top slice. (b) Center slice. (c) Bottom slice.

400

The authors have no conflicts to disclose

TABLE I. Simulation parameters of the proposed brain PET

	Parameters
Crystal material	LYSO
Crystal size (mm^3)	$2\times2\times20$
Inradius (cm)	15
Circumradius (cm)	18.8
Angle between adjacent faces (degree)	116.6
Open face inscribed circle radius (cm)	9.28
Energy window (keV)	250-750
Energy resolution	14%
Coincidence timing window (ns)	6

TABLE II. Digital phantoms. D stands for diameter. L stands for axis length.

Phantom	Physical dimensions (mm)	Application
Cylinder	D: 245 L: 190[13]	Sensitivity
Hemisphere	D: 228[17]	NECR
Point sources	D: 1	Spatial resolution
Derenzo	D: 2.4, 3.4, 5.0, 6.6, 8.4, 9.8	Spatial resolution
Jaszczak	D: 14.4, 19.2, 27.2, 33.6, 43.2, 59.2	Contrast/Noise
Hoffman	Sagittal: 224, Coronal: 224, Vertical: 180	Image visualization

TABLE III. Sensitivities of different geometries

System	Sensitivity	Scatter fraction
HRRT PET	1.04%	36.24%
Helmet	3.58% [13]	31.20% [13]
Dodecahedral PET	6.15%	33.90%

TABLE IV. Peak NECR comparison

Model	HRRT	Helmet-chin	Dodecahedral
NECR(kcps)	307.1	265.0[14]	691.2

TABLE V. CRC at contrast level of 3:1

|	14.4 mm	19.2 mm	27.2 mm	33.6 mm	43.2 mm	59.2 mm
HRRT (%)	60.39	65.46	66.04	68.69	69.23	71.69
Dodecahedral (%)	68.95	70.47	71.60	74.39	79.64	83.38
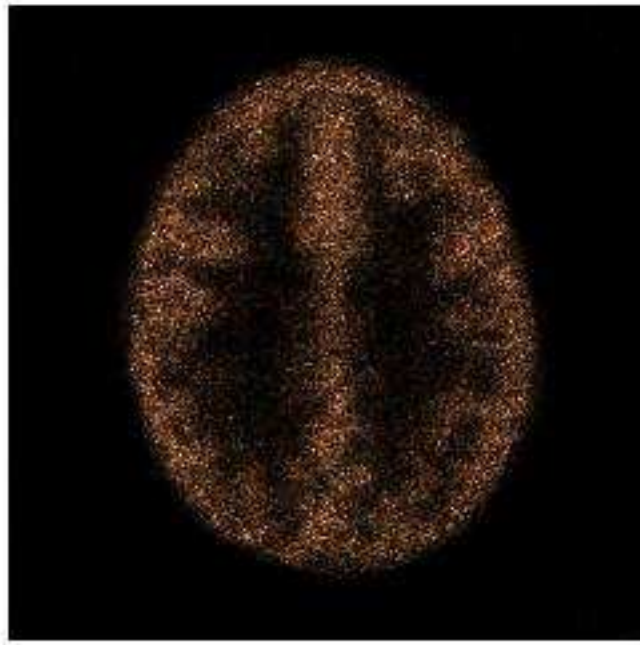
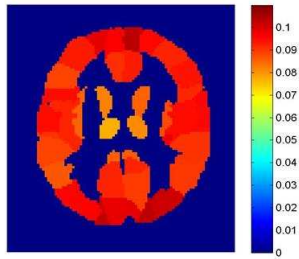mp_12996_f9a1.jpg

mp_12996_f9a2.jpg

mp_12996_f9b1.jpg
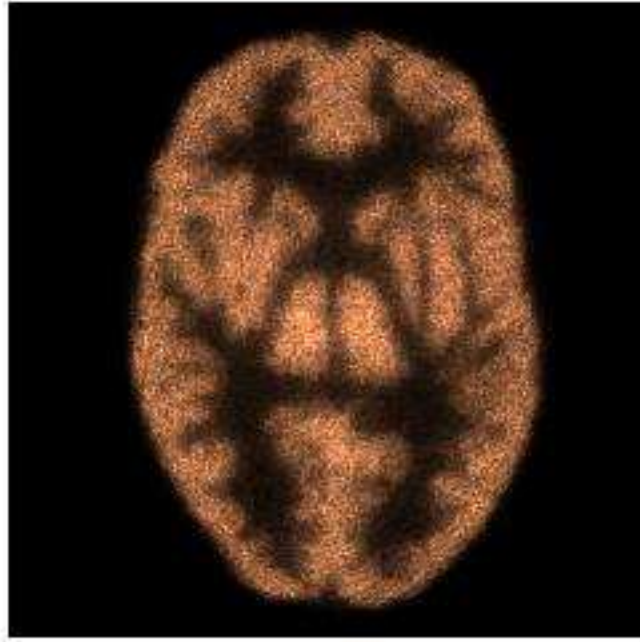
mp_12996_f9b2.jpg
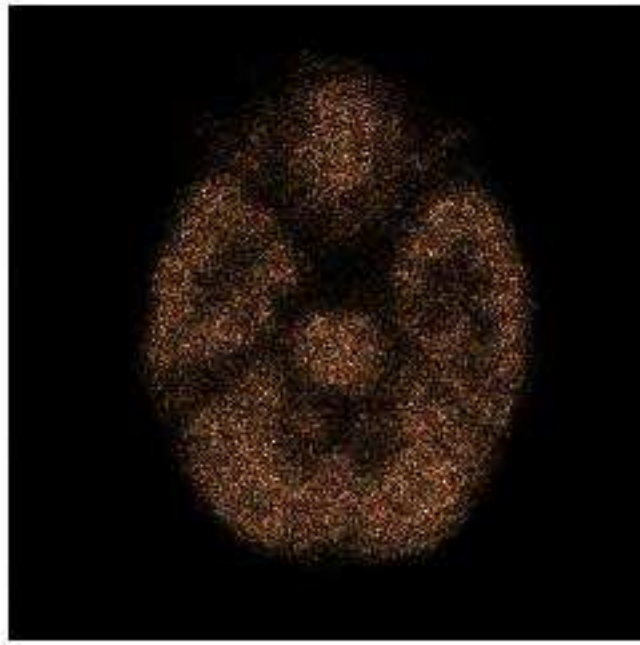
mp_12996_f9c1.jpg
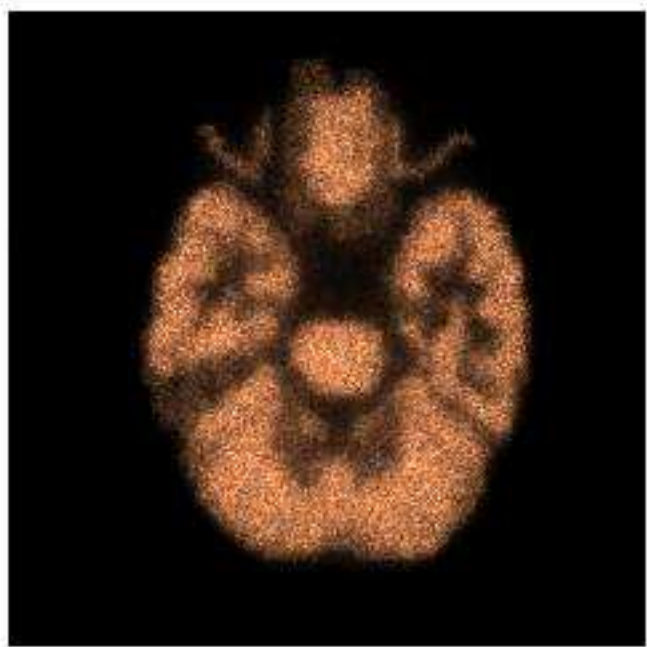
mp_12996_f9c2.jpg
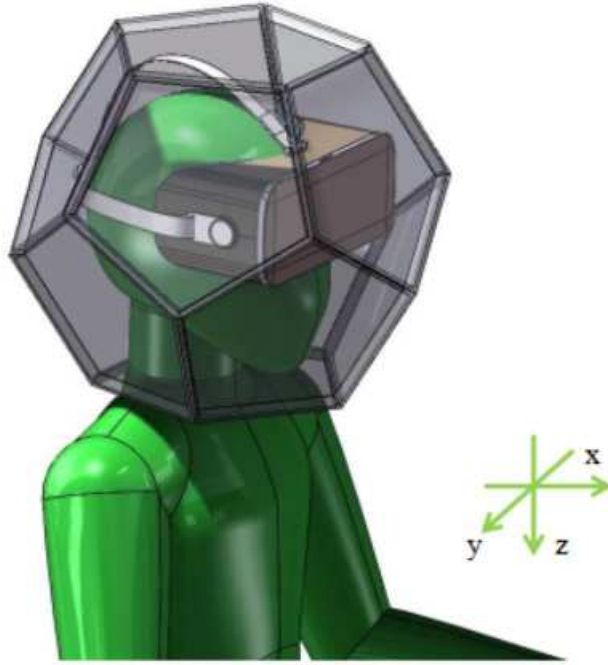
mp_12996_f1a.jpg

mp_12996_f1b.jpg
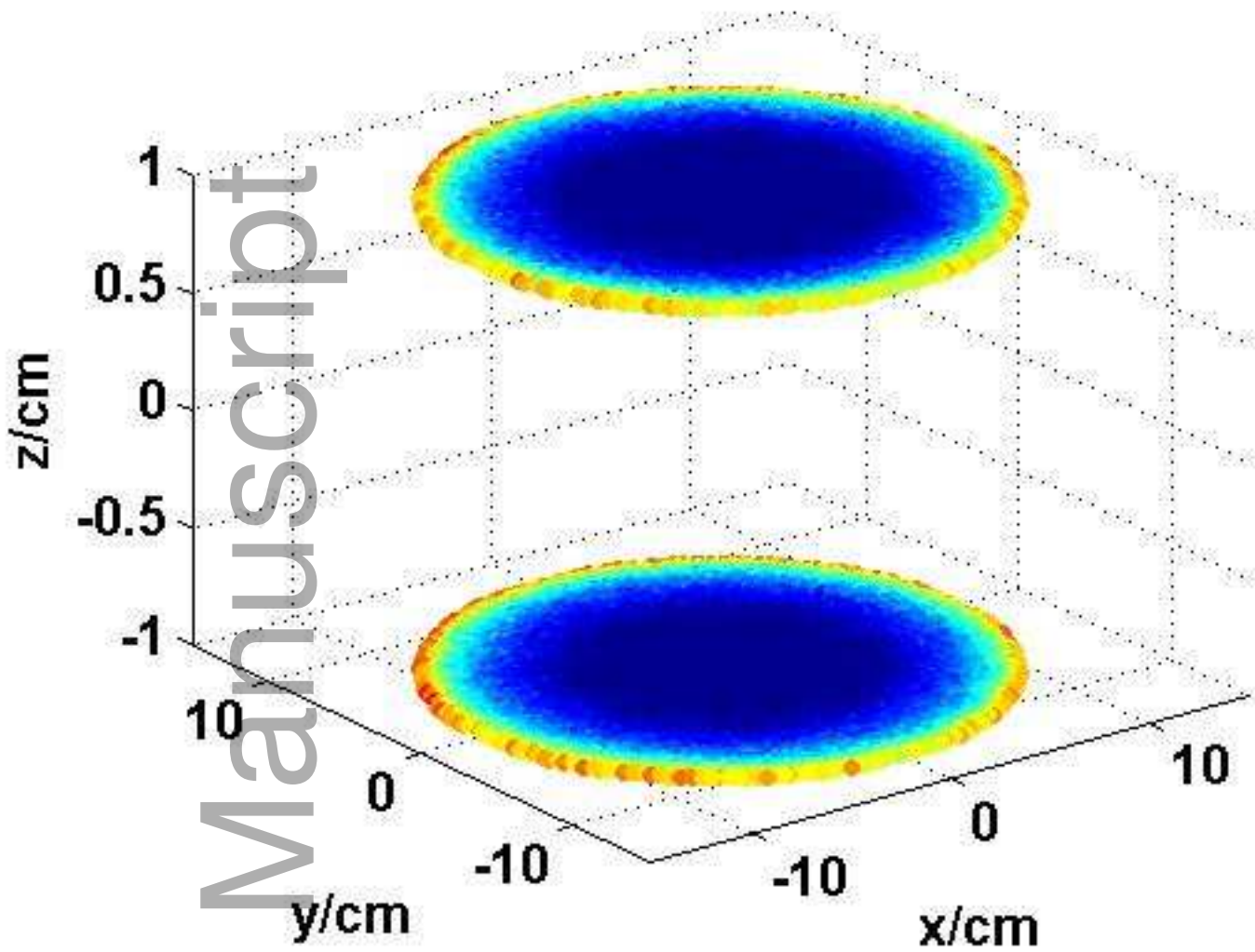
mp_12996_f2a.jpg
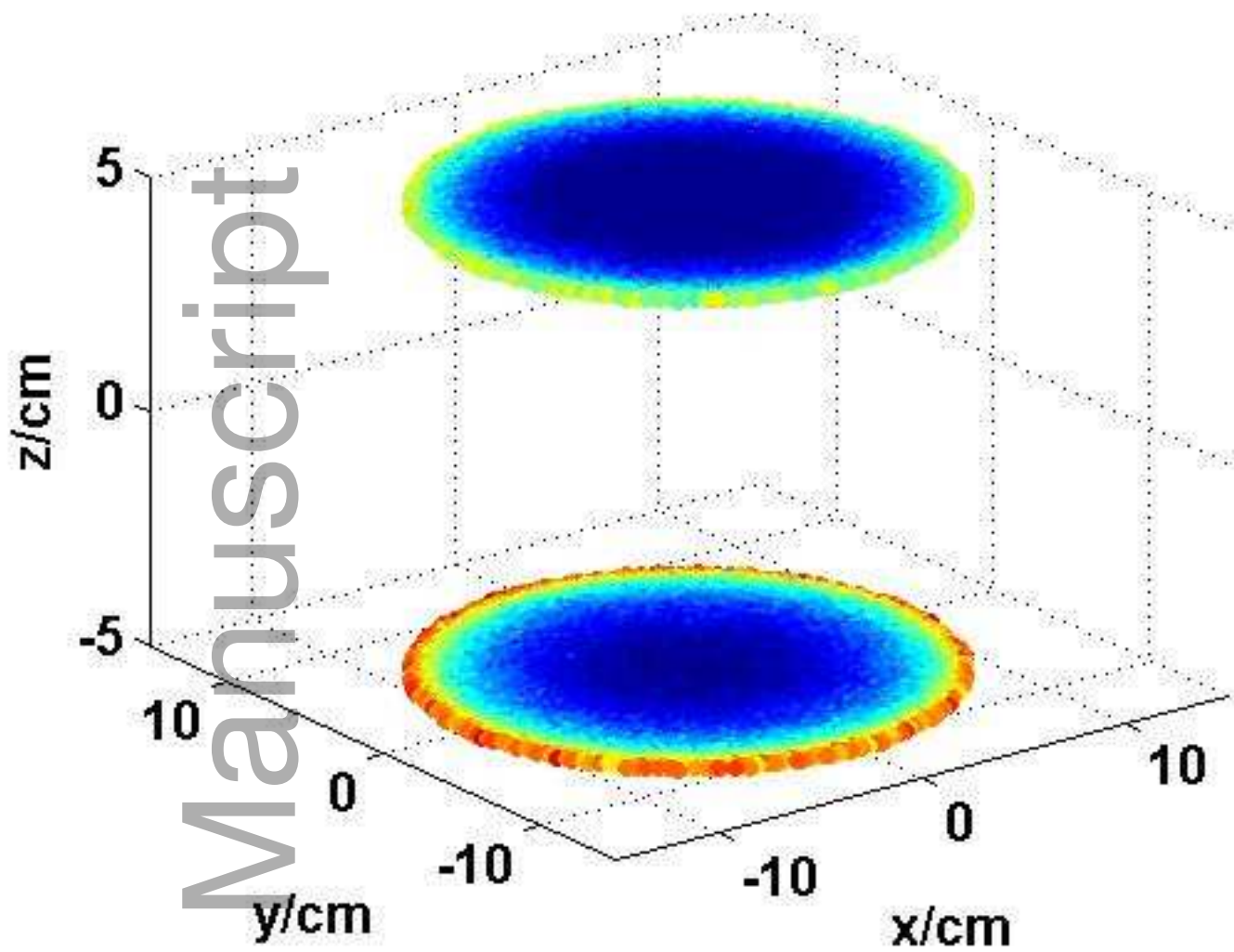
mp_12996_f2b.jpg
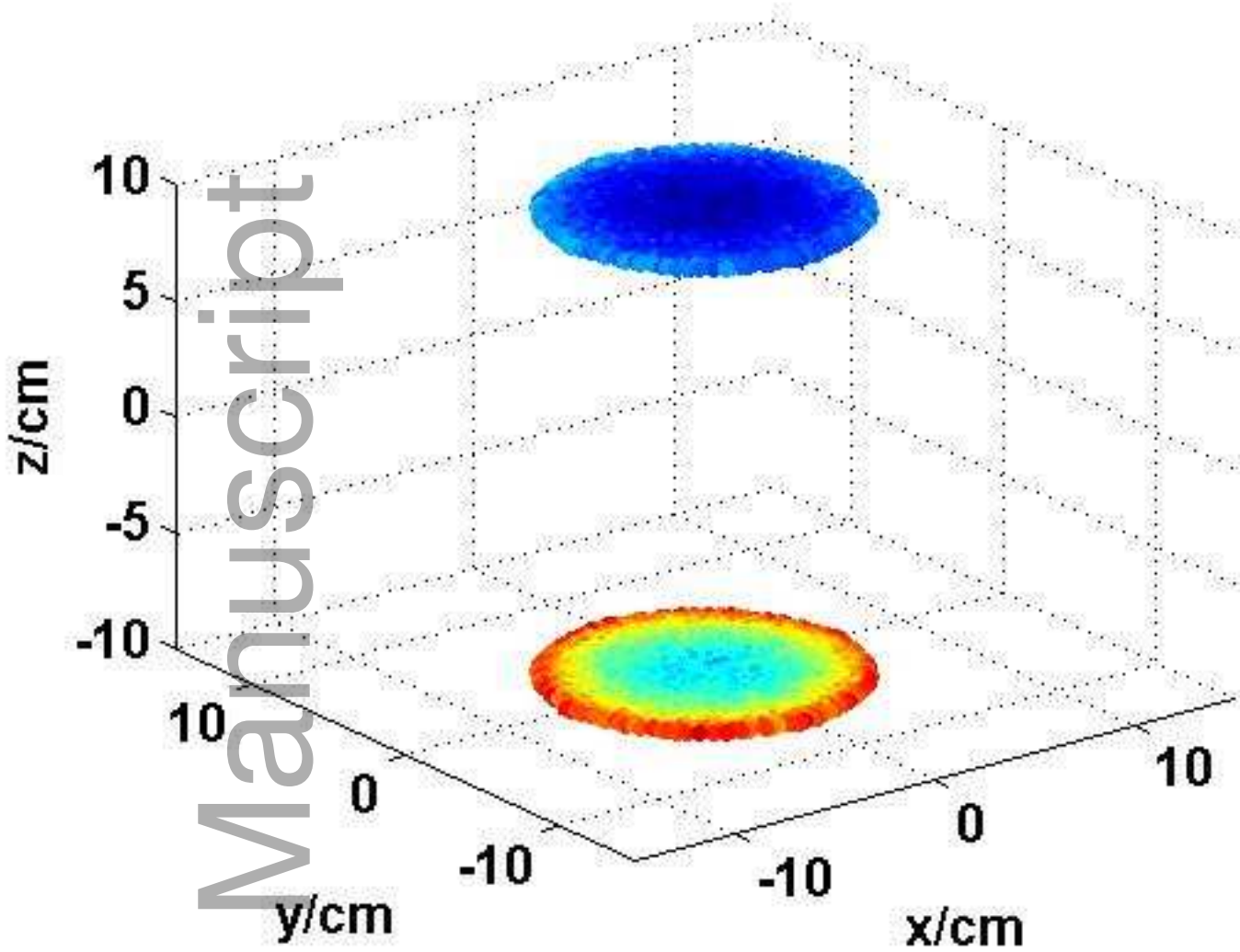
mp_12996_f2c.jpg
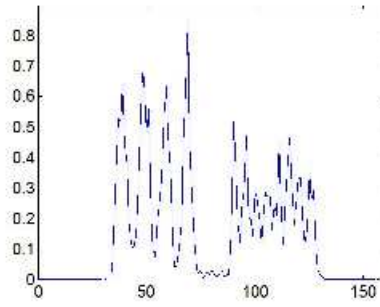
mp_12996_f5a.jpg

mp_12996_f5b.jpg
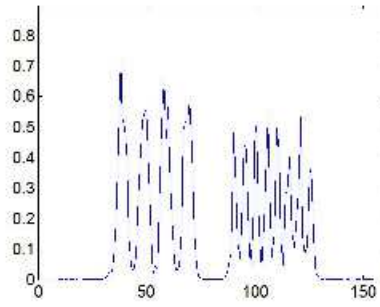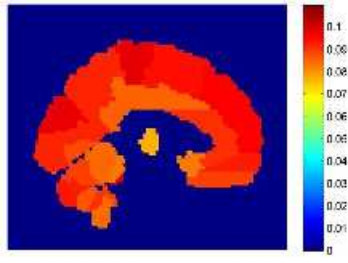
mp_12996_f5c.jpg

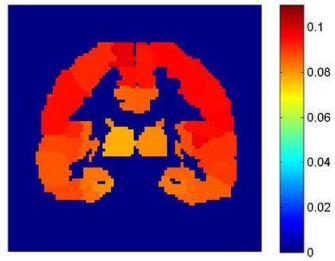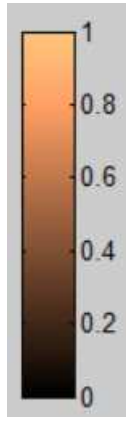mp_12996_f5d.jpg
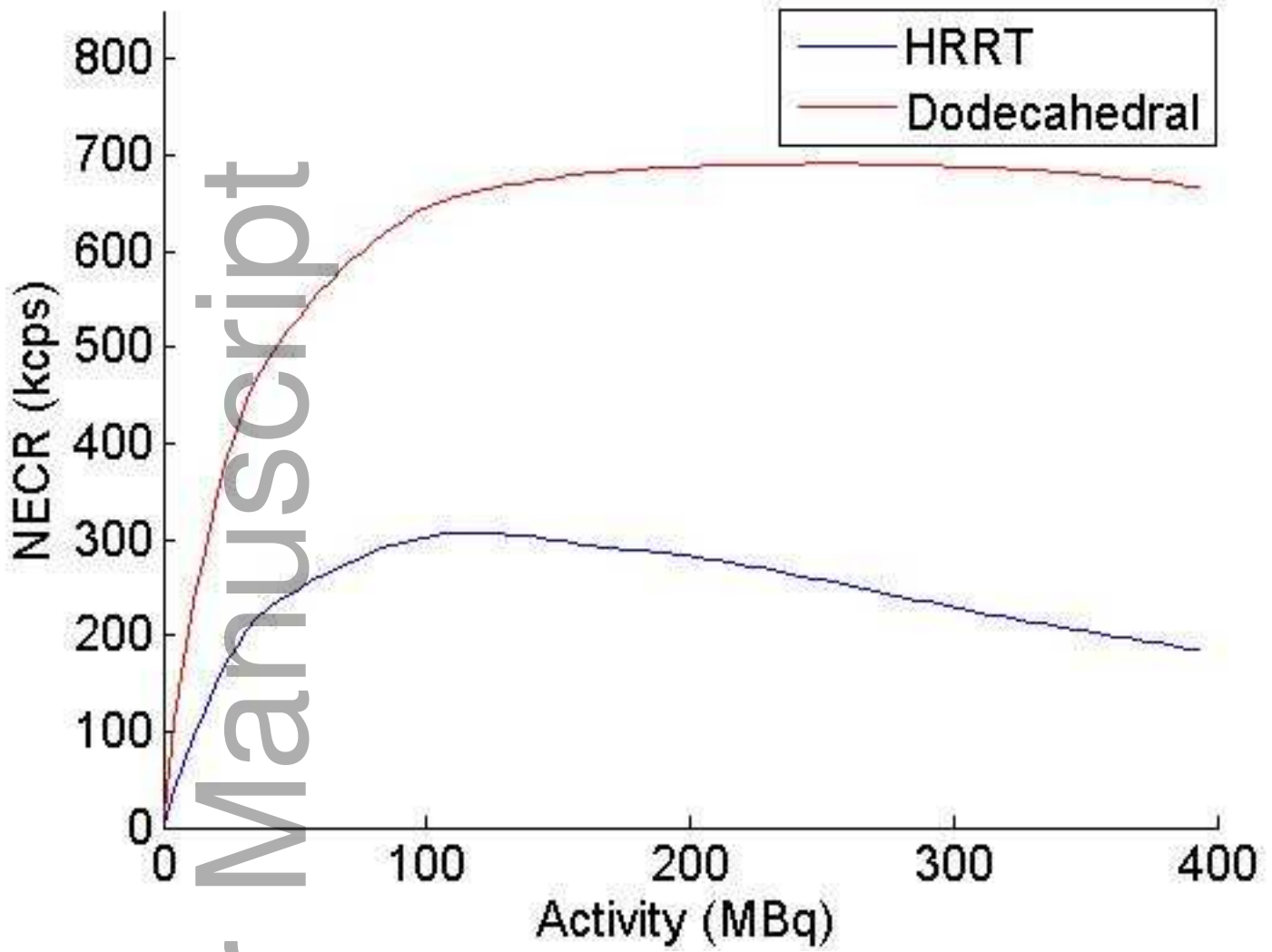
mp_12996_f6.jpg
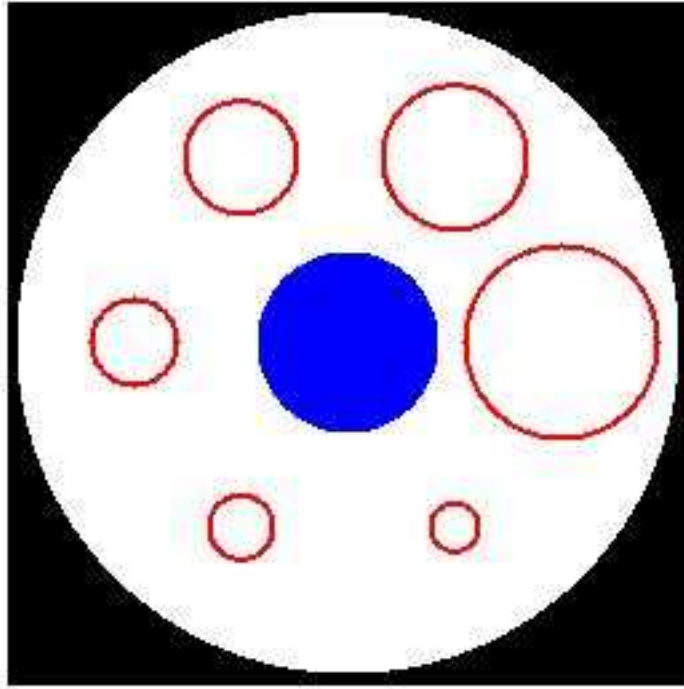
mp_12996_f7a.jpg

mp_12996_f8a.jpg

mp_12996_f8b.jpg

mp_12996_f8c.jpg

mp_12996_f9.jpg